

Secular evolution of viscous and self-gravitating circumstellar discs

E. I. Vorobyov^{1,2*}, Shantanu Basu³

¹*The Institute for Computational Astrophysics, Saint Mary's University, Halifax, NS, B3H 3C3, Canada*

²*Institute of Physics, South Federal University, Rostov-on-Don, 344090, Russia*

³*Department of Physics and Astronomy, University of Western Ontario, London, Ontario, N6A 3K7, Canada*

31 October 2018

ABSTRACT

We add the effect of turbulent viscosity via the α -prescription to models of the self-consistent formation and evolution of protostellar discs. Our models are non-axisymmetric and carried out using the thin-disc approximation. Self-gravity plays an important role in the early evolution of a disc, and the later evolution is determined by the relative importance of gravitational and viscous torques. In the absence of viscous torques, a protostellar disc evolves into a self-regulated state with disk-averaged Toomre parameter $Q \sim 1.5 - 2.0$, non-axisymmetric structure diminishing with time, and maximum disc-to-star mass ratio $\xi = 0.14$. We estimate an effective viscosity parameter α_{eff} associated with gravitational torques at the inner boundary of our simulation to be in the range $10^{-4} - 10^{-3}$ during the late evolution. Addition of viscous torques with a low value $\alpha = 10^{-4}$ has little effect on the evolution, structure, and accretion properties of the disc, and the self-regulated state is largely preserved. A sequence of increasing values of α results in the discs becoming more axisymmetric in structure, being more gravitationally stable, having greater accretion rates, larger sizes, shorter lifetimes, and lower disc-to-star mass ratios. For $\alpha = 10^{-2}$, the model is viscous-dominated and the self-regulated state largely disappears by late times. The axisymmetry and low surface density of this model may contrast with observations and pose problems for planet formation models. The use of $\alpha = 0.1$ leads to very high disc accretion rates and rapid (within 2 Myr) depletion of the disc, and seems even less viable observationally. Furthermore, only the non-viscous-dominated models with low values of $\alpha = 10^{-4} - 10^{-3}$ can account for an early phase of quiescent low accretion rate $\dot{M} \sim 10^{-8} M_{\odot} \text{ yr}^{-1}$ (interspersed with accretion bursts) that can explain the recently observed Very Low luminosity Objects (VeLLOs). We also find that a modest increase in disc temperature caused by a stiffer barotropic equation of state ($\gamma = 1.67$) has little effect on the disc accretion properties averaged over many disc orbital periods ($\sim 10^4$ yr), but can substantially influence the instantaneous mass accretion rates, particularly in the early embedded phase of disc evolution.

Key words: accretion, accretion discs - hydrodynamics - instabilities - ISM: clouds - stars: formation

1 INTRODUCTION

We have recently demonstrated that disc gravity plays an important role not only in the early embedded phase of disc evolution but also in the late accretion phase (Vorobyov & Basu 2007, 2008). In the early embedded phase, when the infall of matter from the surrounding envelope is substantial, mass is transported inward by the gravitational torques from spiral arms that are a manifes-

tation of the envelope-induced gravitational instability in the disc. In the late accretion phase, when the gas reservoir of the envelope is depleted, the distinct spiral structure is replaced by ongoing irregular nonaxisymmetric density perturbations. These perturbations produce a residual nonzero gravitational torque in the disc. In particular, the net gravitational torque in the inner disc tends to be negative during first several million years of the evolution, while the outer disc has a net positive gravitational torque. This is a fundamental property of self-gravitating circumstellar discs around low-mass stars. There is also an overall net

* E-mail: vorobyov@ap.smu.ca (EIV); basu@astro.uwo.ca (SB)

negative torque in the disc that is related to the removal of angular momentum by gas that is accreted in to the central object. Although we do not model the gas flow within a central sink of size 5 AU, the angular momentum that is carried in to this region may be lost to the system via additional processes including magnetic braking and outflows, thereby allowing the gas to reach the central star.

In this paper we seek to determine the effect of *other* mechanisms of radial mass and angular momentum transport on the secular evolution of self-consistently formed circumstellar discs. It is well known that standard collisional viscosity (molecular viscosity) is negligible in application to circumstellar discs. The best candidate to date is turbulent viscosity induced by the magneto-rotational instability (MRI) (Balbus & Hawley 1991), though other mechanisms such as nonlinear hydrodynamic turbulence cannot be completely eliminated due to the large Reynolds numbers involved (e.g. Afshordi et al. 2005). We make no specific assumptions about the source of turbulence and parameterize the magnitude of turbulent viscosity using the usual α -prescription (Shakura & Sunyaev 1973)

$$\nu = \alpha c_s H, \quad (1)$$

where c_s is the sound speed and H is the disc scale height. The most appropriate value of the parameter α in circumstellar discs is uncertain. Both the shearing box and global numerical simulations of the MRI tend to yield the values of α that vary significantly from model to model and range between 10^{-4} and a few $\times 10^{-1}$ (e.g. Hawley et al. 1995; Fleming & Stone 2003; Brandenburg et al. 1996; Stone et al. 1996; Armitage 1998). Motivated by these studies, we have adopted a similar range of values for α . We also assume that α is spatially and temporally constant, i.e. it represents a mean value, time-averaged over many orbital periods of the disc. Radial variations in α may (and should) be present in the disc but it requires a more thorough consideration of the disc physics and is left for a follow-up paper.

Our study of the self-consistent formation and long-term evolution of circumstellar discs has been preceded by numerical simulations of Lin & Pringle (1990); Nakamoto & Nakagawa (1995); Hueso & Guillot (2005) and others. However, our work is different in one important aspect – we employ a fully two-dimensional numerical hydrodynamics simulations in the thin-disc approximation (in contrast to earlier one-dimensional studies). As a result, we account for disc self-gravity self-consistently by solving the Poisson integral (see Vorobyov & Basu 2006) and need not parameterize gravitational torques in terms of the α -prescription. Use of the thin-disc approximation is, unfortunately, a necessity. Fully three-dimensional numerical simulations are too computationally expensive to study the disc evolution on time scales of several Myr.

The paper is organized as follows. Section 2 gives a brief description of model equations and initial conditions. The main results are presented in Section 3. The observational implications and comparison with earlier studies are discussed in Section 5. The main conclusions are summarized in Section 6.

2 MODEL DESCRIPTION

We use the thin-disc approximation to compute the evolution of non-axisymmetric rotating, gravitationally bound cloud cores. We start our numerical integration in the pre-stellar phase, which is characterised by a collapsing *starless* cloud core, and continue into the late accretion phase, which is characterised by a protostar/disc system. This ensures a *self-consistent* formation of circumstellar discs in our numerical simulations. Once the disc is formed, its subsequent evolution is determined by an interplay between the efficiency of the mass and angular momentum transport in the disc¹ and the infall rate of matter from the surrounding envelope onto the disc. The disc-envelope interaction is taken into account self-consistently, since we evolve numerically the disc and envelope altogether. It means that there is no source term in the numerical grid allowing for mass deposition from the envelope, but the mass infall rate onto the disc is actually determined by the dynamics of gas in the envelope. The disc occupies the innermost regions of our numerical grid and the envelope occupies the rest of the grid. We note the infall rate of matter from the envelope onto the disc is not necessarily the same as the mass accretion rate from the disc onto the protostar. While the former shows a fast decline with time, the latter is usually characterized by a much slower decline and has a strong dependence on the stellar mass (Vorobyov & Basu 2007, 2008).

For details of the basic equations, numerical methods and numerical tests we refer the reader to Vorobyov & Basu (2006). Here we briefly provide the basic equations modified to include the effect of viscosity. The basic equations of mass and momentum transport in the thin-disc approximation are

$$\frac{\partial \Sigma}{\partial t} = -\nabla_p \cdot (\Sigma \mathbf{v}_p), \quad (2)$$

$$\Sigma \frac{d\mathbf{v}_p}{dt} = -\nabla_p \mathcal{P} + \Sigma \mathbf{g}_p + (\nabla \cdot \mathbf{\Pi})_p, \quad (3)$$

where Σ is the mass surface density, $\mathcal{P} = \int_{-Z}^Z P dz$ is the vertically integrated form of the gas pressure P , Z is the radially and azimuthally varying vertical scale height, $\mathbf{v}_p = v_r \hat{\mathbf{r}} + v_\phi \hat{\boldsymbol{\phi}}$ is the velocity in the disc plane, $\mathbf{g}_p = g_r \hat{\mathbf{r}} + g_\phi \hat{\boldsymbol{\phi}}$ is the gravitational acceleration in the disc plane, and $\nabla_p = \hat{\mathbf{r}} \partial / \partial r + \hat{\boldsymbol{\phi}} r^{-1} \partial / \partial \phi$ is the gradient along the planar coordinates of the disc. We note that \mathbf{g}_p includes the input from the central star when it forms. The viscous stress tensor $\mathbf{\Pi}$ is expressed as

$$\mathbf{\Pi} = 2\Sigma \nu \left(\nabla v - \frac{1}{3} (\nabla \cdot \mathbf{v}) \mathbf{e} \right), \quad (4)$$

where ∇v is a symmetrized velocity gradient tensor, \mathbf{e} is the unit tensor, and ν is the kinematic viscosity. The components of $(\nabla \cdot \mathbf{\Pi})_p$ in polar coordinates (r, ϕ) are given in the Appendix. We emphasize that we do not take any simplifying assumptions about the form of the viscous stress tensor, apart from those imposed by the adopted thin-disc approximation. It can be shown (Lodato 2008) that equation (3) can be reduced to the usual equation for the conservation of

¹ In fact, discs may also transport angular momentum to the external environment due to magnetic braking. This effect will be considered in a follow-up paper.

angular momentum of a radial annulus in the axisymmetric viscous accretion disc (Pringle 1981).

Equations (2) and (3) are closed with a barotropic equation that makes a smooth transition from isothermal to adiabatic evolution at $\Sigma = \Sigma_{\text{cr}} = 36.2 \text{ g cm}^{-2}$:

$$\mathcal{P} = c_s^2 \Sigma + c_s^2 \Sigma_{\text{cr}} \left(\frac{\Sigma}{\Sigma_{\text{cr}}} \right)^\gamma, \quad (5)$$

where $c_s = 0.188 \text{ km s}^{-1}$ is the sound speed in the beginning of numerical simulations and $\gamma = 1.4$. Equation (5), though neglecting detailed cooling and heating processes, was shown to reproduce to a first approximation the radial temperature gradients in circumstellar discs (Vorobyov & Basu 2007) and the density-temperature relation in collapsing cloud cores (Vorobyov & Basu 2006).

It should be stressed here that circumstellar discs described by the barotropic equation of state with $\gamma = 1.4$ are susceptible to fragmentation and formation of stable clumps in the early embedded phase of evolution. A more accurate treatment of the energy balance in the disc involving radiative cooling from the disc surface and shock heating due to artificial viscosity has shown that the strength of gravitational instability in general and the disc propensity to fragmentation in particular depend on the rate of cooling (e.g. Gammie 2001; Johnson & Gammie 2003; Rice et al. 2003; Lodato & Rice 2004; Mejía et al. 2005). In addition, fragmentation can be stabilized in the inner discs by slow cooling (e.g. Stamatellos & Whitworth 2008) and in the outer discs by stellar and envelope irradiation (Matzner & Levin 2005; Cai et al. 2008). However, recent semi-analytical and numerical studies (including radiation transfer) reveal clump formation in discs (particularly, in their outer parts) around stars with mass equal to or more massive than one solar mass (Krumholz et al. 2007; Mayer et al. 2007; Stamatellos et al. 2007; Boss 2008; Kratter et al. 2008). These simulations produce discs that are usually hotter than those described by a barotropic equation of state with $\gamma = 1.4$ but that does not necessarily imply less efficient transport due to gravitational torques. As Cai et al. (2008) have demonstrated, a modest rise in the disc temperature (from the envelope irradiation) may in fact promote transport due to a growing relative strength of low-order spiral modes ($m \leq 2$) in the disc. In order to examine if a higher disc temperature can affect our main results, we consider a stiffer barotropic equation of state with $\gamma = 1.67$ in Section 4.

The kinematic viscosity is computed during numerical simulations as

$$\nu = \alpha \tilde{c}_s Z, \quad (6)$$

where $\tilde{c}_s^2 = \partial \mathcal{P} / \partial \Sigma$ is the effective sound speed of (generally) non-isothermal gas. The vertical scale height Z is determined in each computational cell using an assumption of local hydrostatic equilibrium in the gravitational field of the central star and the disc (see Appendix A).

The initial conditions are similar to those in Vorobyov & Basu (2007). The initial radial surface density and angular velocity profiles of the model cloud core with mass $0.8 M_\odot$ and mean molecular weight 2.33 are characteristic of a collapsing axisymmetric magnetically supercritical core (Basu 1997):

$$\Sigma = \frac{r_0 \Sigma_0}{\sqrt{r^2 + r_0^2}}, \quad (7)$$

$$\Omega = 2\Omega_0 \left(\frac{r_0}{r} \right)^2 \left[\sqrt{1 + \left(\frac{r}{r_0} \right)^2} - 1 \right]. \quad (8)$$

The scale length $r_0 = kc_s^2 / (G\Sigma_0)$, where $k = \sqrt{2}/\pi$ and $\Sigma_0 = 0.12 \text{ g cm}^{-2}$. The central angular velocity is $\Omega_0 = 1.1 \text{ km s}^{-1} \text{ pc}^{-1}$. We have adopted a somewhat higher value of Ω_0 than in Vorobyov & Basu (2007) in order to emphasize the burst phase of mass accretion. Our adopted initial profiles are characterized by the important dimensionless free parameter $\eta \equiv \Omega_0^2 r_0^2 / c_s^2$. The asymptotic ($r \gg r_0$) ratio of centrifugal to gravitational acceleration has magnitude $\sqrt{2}\eta$ (see Basu 1997) and the centrifugal radius of a mass shell initially located at radius r is estimated to be $r_{\text{cf}} = j^2 / (Gm) = \sqrt{2}\eta r$. For our chosen parameters, we find $\eta = 1.42 \times 10^{-3}$, and $r_{\text{cf}} = 16.6 \text{ AU}$ for the outermost mass shell located initially at $r_{\text{out}} = 0.04 \text{ pc}$.

Equations (2), (3), (5) are solved in polar coordinates (r, ϕ) on a numerical grid with 128×128 points. We use the method of finite differences with a time-explicit, operator-split solution procedure. Advection is performed using the second-order van Leer scheme. The radial points are logarithmically spaced. The innermost grid point is located at $r = 5 \text{ AU}$, and the size of the first adjacent cell is 0.3 AU . We introduce a “sink cell” at $r < 5 \text{ AU}$, which represents the central star plus some circumstellar disc material, and impose a free inflow inner boundary condition. The outer boundary is reflecting. The gravity of a thin disc is computed by directly summing the input from each computational cell to the total gravitational potential. The convolution theorem is used to speed up the summation. A small amount of artificial viscosity is added to the code, though the associated artificial viscosity torques were shown to be negligible in comparison with gravitational torques (Vorobyov & Basu 2007). A more detailed explanation of numerical methods and relevant tests can be found in Vorobyov & Basu (2006, 2007).

3 RESULTS

We consider five models, each having identical initial conditions but distinct values of spatially and temporally uniform α . In particular, model 1 is characterized by $\alpha = 0$ and is used as the standard model against which other models with non-zero viscosity are compared. Models 2, 3, 4, and 5 have α equal to 10^{-4} , 10^{-3} , 10^{-2} , and 10^{-1} , respectively. To facilitate the comparison between viscous and non-viscous models, α is kept zero in the early evolution in all models and is set to its corresponding value only after the disc is formed at $t \approx 0.14 \text{ Myr}$.

3.1 Radial profiles

Solid lines in Figs 1-4 show three distinct snapshots in the evolution of a circumstellar disc in model 2 (Fig. 1), model 3 (Fig. 2), model 4 (Fig. 3), and model 5 (Fig. 4). The numbers in the top horizontal row indicate ages of the disc, t_{disc} . Horizontal rows in each figure show (from top to bottom) the *azimuthally averaged* radial profiles of angular velocity $\bar{\Omega}$, surface density $\bar{\Sigma}$, temperature \bar{T} , Toomre \bar{Q} -parameter, and the relative surface density perturbation $\Delta\Sigma$. Dashed lines in each figure give the corresponding radial profiles for

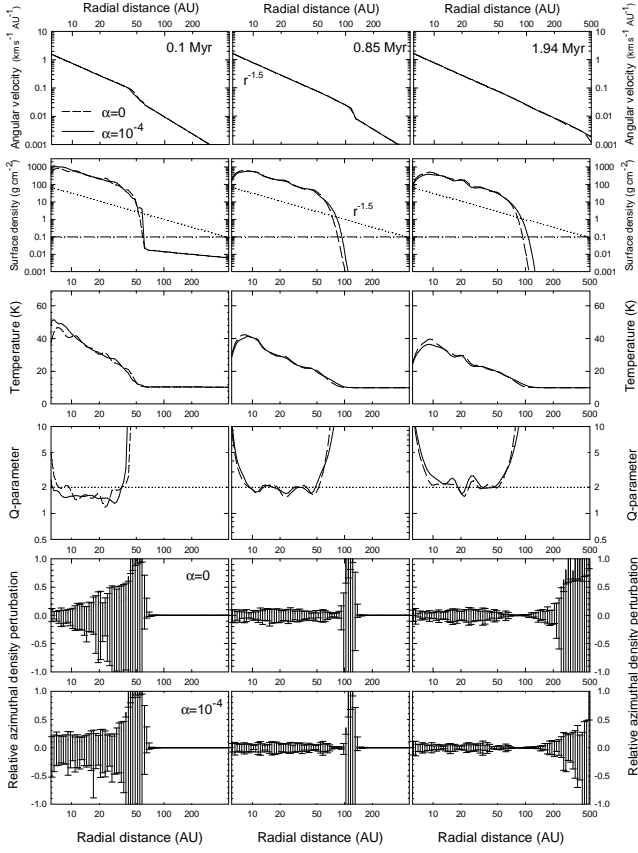


Figure 1. Radial structure of the circumstellar disc in the $\alpha = 0$ model 1 (dashed lines) and $\alpha = 10^{-4}$ model 2 (solid lines). Top to bottom: azimuthally averaged values of $\bar{\Omega}$, $\bar{\Sigma}$, \bar{T} , \bar{Q} , and $\Delta\Sigma$ in the 0.1-Myr-old disc (left-hand column), 0.85-Myr-old disc (middle column) and 1.94-Myr-old disc (right-hand column). The error bars in two bottom rows show the minimum and maximum $\Delta\Sigma(r_i, \phi_i)$ in each radial annulus. The dotted lines in the second row show the surface density as inferred from the minimum mass solar nebula model, and the dot-dashed lines mark a fiducial critical density (1.0 g cm^{-2}) for transition between the disc and envelope.

the $\alpha = 0$ model 1. The Toomre parameter is calculated as $Q = \tilde{c}_s \Omega / (\pi G \Sigma)$. In each computational zone (r_i, ϕ_j) we calculate the relative azimuthal perturbation to the surface density

$$\Delta\Sigma(r_i, \phi_j) = \frac{\Sigma(r_i, \phi_j) - \frac{1}{N} \sum_{j=1}^N \Sigma(r_i, \phi_j)}{\Sigma(r_i, \phi_j)}, \quad (9)$$

where N is the number of grid zones in the azimuthal direction. The error bars in two bottom rows of Figs 1-4 show the minimum and maximum $\Delta\Sigma(r_i, \phi_i)$ in each radial annulus.

It is evident that $\alpha = 10^{-4}$ (Fig. 1) has little effect on the secular evolution of a self-gravitating disc. In the end of numerical simulations, when the disc is 1.94-Myr-old, the radial profiles of the viscous and non-viscous models are nearly identical. The maximum disc radius is about 100 AU^2 and both the angular velocity and surface density scale as $r^{-3/2}$. In the early evolution ($t_{\text{disc}} = 0.1 \text{ Myr}$), the disc is

² The disc is defined as the radial distance at which the surface density drops below 0.1 g cm^{-2}

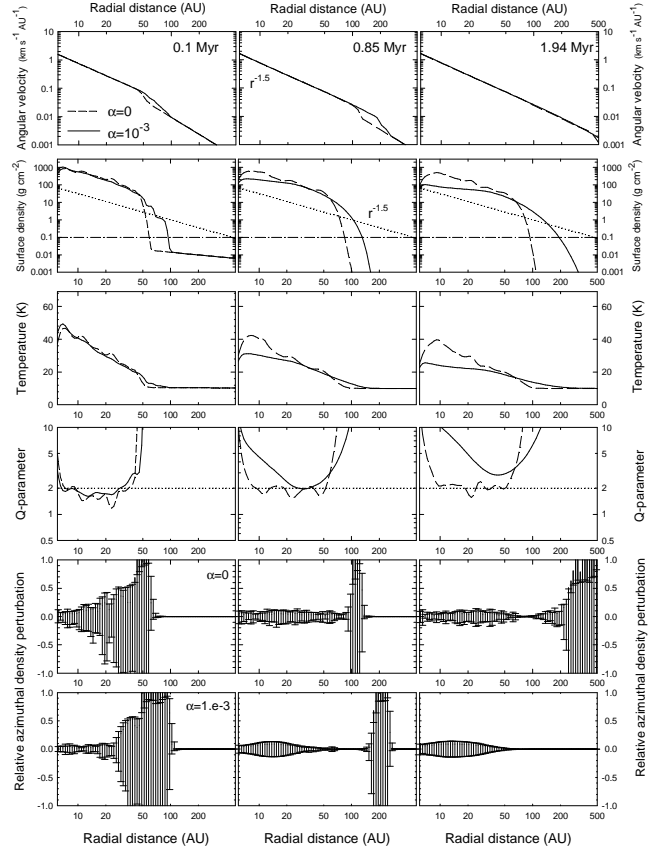


Figure 2. Radial structure of the circumstellar disc in the $\alpha = 0$ model 1 (dashed lines) and $\alpha = 10^{-3}$ model 3 (solid lines). See captions to Fig. 1 for details.

prone to gravitational instability as indicated by both the low values of $Q = 1.2 - 1.7$ and large-amplitude azimuthal density perturbations $\Delta\Sigma = 0.2 - 1.0$. In the late evolution ($t_{\text{disc}} \gtrsim 0.85 \text{ Myr}$), the disc regulates itself near the boundary of gravitational stability, $Q = 1.7 - 2.0$. This state is characterized by ongoing low-amplitude density perturbations powered by swing amplification at the disc's sharp outer edge, resembling truncated circumstellar discs seen in young stellar objects. The dotted lines in the surface density panels in Figures 1-4 show the radial surface density profile as expected from the minimum mass solar nebula (MMSN) model, $\Sigma_{\text{mmsn}} = 10^3 (r/\text{AU})^{-3/2} \text{ g cm}^{-2}$ (Weidenschilling 1977). Our model disc is approximately a factor of ten more dense than the MMSN. This implies that most of the disc is actually in the optically *thick* regime, which may have important consequences for the disc mass measurements in T Tauri stars (Andrews & Williams 2005).

As the magnitude of α is increased to 10^{-3} (Fig. 2), numerical simulations start to show noticeable differences between viscous and non-viscous discs in the late evolution ($t_{\text{disc}} \gtrsim 0.85 \text{ Myr}$). In particular, the disc starts to spread out and its sharp outer edge is replaced with a shallow tail. The disc radius at $t_{\text{disc}} = 1.94 \text{ Myr}$ is twice as large in model 3 ($\approx 200 \text{ AU}$) as that in the non-viscous model 1. Both Σ and T decrease throughout the disc. In contrast to non-viscous discs, the radial surface density profile in model 3 cannot be fitted by a single slope. In particular, Σ scales as $r^{-0.8}$ in the radial range $5 - 60 \text{ AU}$ but becomes progressively

steeper in the outer portion of the disc. It is also worth noting that viscous discs start to slowly drift apart from a self-regulation state characterized by a near constant $Q \approx 1.7 - 2.0$. For example, the minimum Q value in model 3 at $t_{\text{disc}} = 1.94$ Myr is 2.8.

As we continue to increase the value of α to 10^{-2} (Fig. 3), the long-term effect of viscosity on the disc evolution becomes more profound. It is only the early phases of evolution in model 4 ($t_{\text{disc}} = 0.1$ Myr) that bear some similarities with model 1, the late evolution is considerably different. Figure 3 indicates an overall decrease in the values of Σ as compared to those in the non-viscous model 1, which results in a disc that is optically thin and cold at $t_{\text{disc}} \gtrsim 0.85$ Myr. The values of Σ in the radial range $10 - 200$ AU are similar, within a factor of few, to those of the MMSN (dotted lines) but become lower in the entire disc after 1.0 Myr. It is important to note that planet formation models (e.g. Ida & Lin 2004) require discs with gas surface densities a few times greater than that of the MMSN. The radial surface density profile cannot be characterized by a single slope. It is nearly flat in the inner part of the disc and steepens out in the outer parts. The disc radius amounts to roughly $350 - 400$ AU at $t_{\text{disc}} = 1.94$ Myr, though we note there is no clear disc boundary and the surface density gradually declines with radius to the values typical for molecular cloud cores. The disc is virtually *axisymmetric* in the late evolution, except for a small portion near the inner boundary, and is characterized by $Q \gg 1.0$. This marks the largest and most noticeable difference between the purely self-gravitating disc and the one with $\alpha = 0.01$ – the latter is profoundly gravitationally stable.

The gravitational stabilization of viscous discs along a sequence of increasing α is accompanied by progressively more axisymmetric structure. This is an important point to keep in mind given the available observational data demonstrating that 1-Myr-old discs are non-axisymmetric and show elements of spiral arms and arcs (e.g. Fukagawa et al. 2004; Grady et al. 2001)³. Furthermore, we point out that direct gravitational instability as a scenario for giant planet formation is not viable for the viscous-dominated models.

An increase in α to 10^{-1} (Fig. 4) has a catastrophic effect on the secular evolution of a circumstellar disc. After two million years of evolution, the disc is virtually washed out as a result of a very efficient mass and angular momentum radial transport. In particular, the values of Σ are more than an order of magnitude smaller than those of the MMSN at all radii. The Toomre Q -parameter is much larger than unity and is off the scale in Fig. 4 at $t \gtrsim 0.85$ Myr. Definitely, circumstellar discs cannot sustain such large values of α for a long time without being completely destroyed.

Figs 1-4 show that the angular velocity of the inner disc increases with time only by a few per cent. One may expect this trend be more profound as the star accumulates mass from the disc. However, by the time disc forms in our numerical simulations (~ 0.14 Myr), the star has already gained most of its final mass (see Fig. 6). This is partly caused by a relatively low initial rate of rotation of our cloud

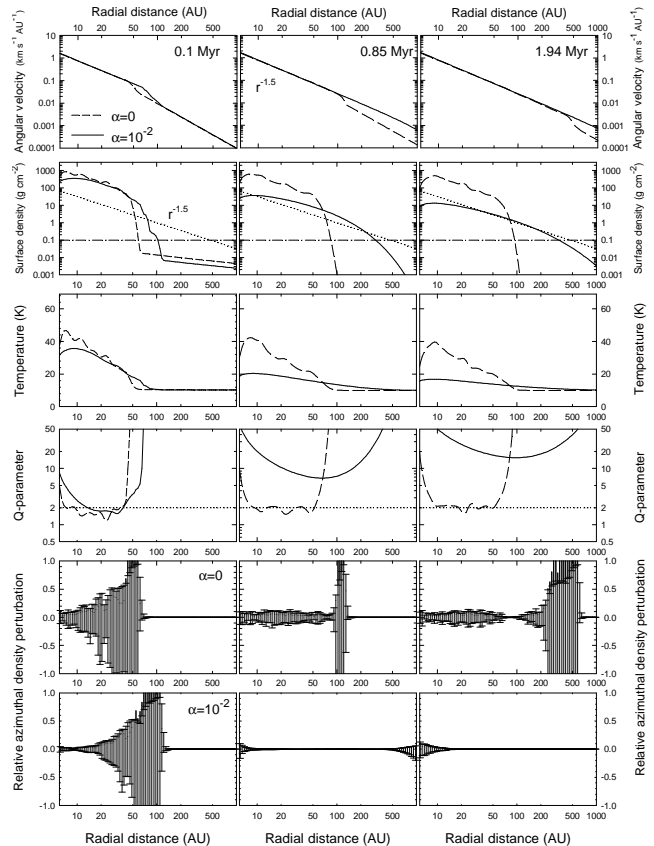


Figure 3. Radial structure of the circumstellar disc in the $\alpha = 0$ model 1 (dashed lines) and $\alpha = 10^{-2}$ model 4 (solid lines). See captions to Fig. 1 for details.

core and partly by the use of a finite-size (5 AU) sink cell in our code. We cannot resolve the very early phases of disc evolution.

3.2 Gravitational torques versus viscous torques

The differences in the secular evolution of models 1 – 4 can be understood if we compare the temporal evolution of gravitational and viscous torques in these models. The blue lines in Figure 5 show the net (positive plus negative) gravitational torque in the disc \mathcal{T}_g , while the red and black lines show the net viscous torque \mathcal{T}_v . The horizontal axis shows time elapsed since the disc formation. Both the gravitational and viscous torques are plotted in *absolute* units and the net gravitational torque is always *negative*. However, the net viscous torque is found to change its sign. In the early disc evolution at $t \lesssim 0.1$ Myr, the net viscous torque is mostly positive and its magnitude is plotted with red. In the subsequent evolution, the net viscous torque becomes negative and its magnitude is plotted with black. The adopted values of α are indicated in each panel. The net gravitational torque \mathcal{T}_g is found by summing all local gravitational torques $\tau_g(r, \phi) = -m(r, \phi) \partial \Phi / \partial \phi$ in each computational cell occupied by the disc, where Φ is the local gravitational potential and $m(r, \phi)$ is the gas mass in a cell with polar coordinates (r, ϕ) . The net viscous torque is found in a similar manner by summing up all local viscous torques $\tau_v(r, \phi) = r (\nabla \cdot \mathbf{\Pi})_\phi S(r, \phi)$, where $S(r, \phi)$ is the surface area

³ Given a large size and relatively low mass of the disc observed in AB Aurigae, the nonaxisymmetry in this case may be triggered by some kind of close encounter.

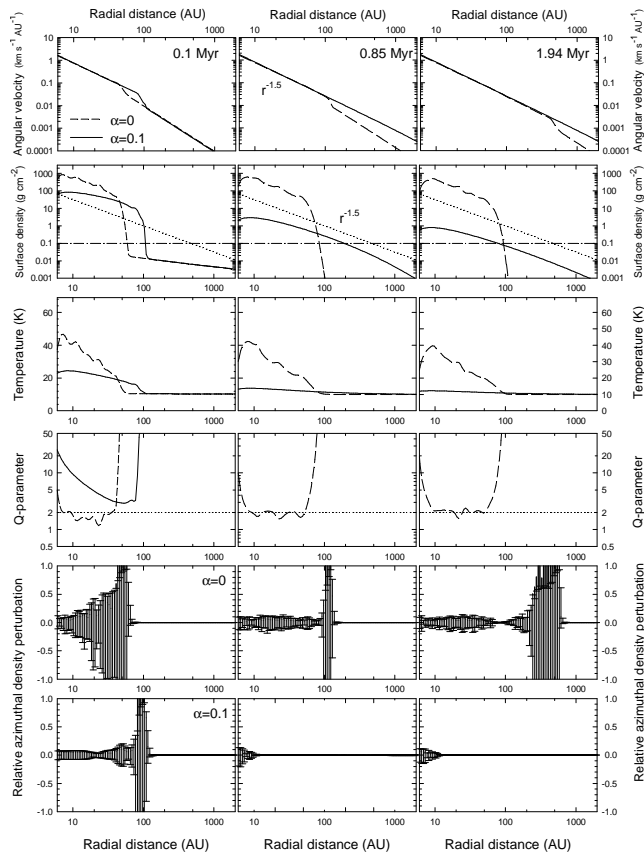


Figure 4. Radial structure of the circumstellar disc in the $\alpha = 0$ model 1 (dashed lines) and $\alpha = 10^{-1}$ model 5 (solid lines). See captions to Fig. 1 for details.

occupied by a cell with polar coordinates (r, ϕ) . The local torques $\tau_g(r, \phi)$ and $\tau_v(r, \phi)$ are actually the local azimuthal components of the corresponding forces, acting on a fluid element with mass $m(r, \phi)$, multiplied by the radius r .

Figure 5 clearly demonstrates that gravitational torques dominate over viscous torques in the $\alpha = 10^{-4}$ model. The difference is particularly large in the early evolution and is decreasing later but \mathcal{T}_g remains at least an order greater than \mathcal{T}_v in the 2-Myr-old disc. A qualitative change in the temporal behaviour of torques is seen in the $\alpha = 10^{-3}$ model – while the early disc evolution ($t \lesssim 0.8$ Myr) is still controlled by gravity, the subsequent evolution is viscosity dominated. This effect is even more prominent in the $\alpha = 10^{-2}$ disc, in which the viscous torques start to prevail already after 0.3 Myr of evolution. This explains profound changes in the disc structure seen in Fig. 3. The $\alpha = 10^{-1}$ model is an extreme case, in which viscous torques compete with those of gravity even in the early evolution and completely prevail in the late evolution.

It is important to note here that gravitational stability properties of astrophysical discs may be modified in the presence of magnetic fields. For instance, Fromang et al. (2004a,b) have demonstrated that the MRI leads to turbulence, which gives rise to a complicated spiral pattern in the disc and lowers the strength of the gravitational stress tensor by a factor of 2 due to the nonlinear mode-mode interaction. In addition, frozen-in magnetic fields tend to decrease the critical Toomre parameter Q_{cr} and the magnetic

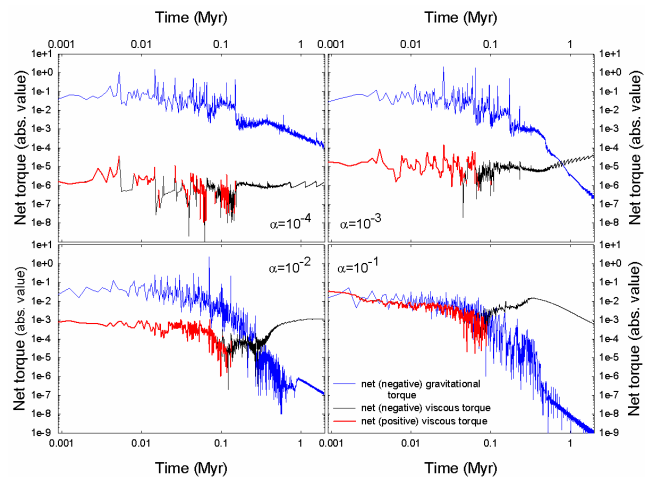


Figure 5. Temporal evolution of gravitational and viscous net torques (in absolute values) in model 2 (upper left), model 3 (upper right), model 4 (lower left), and model 5 (lower right). The horizontal axis shows time elapsed since the disc formation. The net gravitational torque (blue lines) is always negative, while the net viscous torques can be both positive (red lines) and negative (black lines). The torque is measured in units of $8.66 \times 10^{40} \text{ gm cm}^2 \text{ s}^{-2}$.

disc has to attain a lower value of Q in order to destabilize (Vorobyov & Basu 2006). Since α -viscosity is most likely caused by the MRI, we acknowledge that the actual strength of gravitational torques may be somewhat smaller than that shown in Fig. 5. We plan to investigate the effect of magnetic fields and magnetic braking in a follow-up paper.

Two important features in Figure 5 need to be emphasized. First, a decline of gravitational torques with time is mostly caused by a gradual approach of the disc to a stable state. As a consequence, large scale spiral arms in the early phase are replaced with ongoing low-amplitude density perturbations in the late phase (Vorobyov & Basu 2007). As Figure 5 demonstrates, turbulent viscosity expedites the onset of gravitational stability and the $\alpha = 10^{-2} - 10^{-1}$ discs are virtually axisymmetric and gravitationally stable after just 1.0 Myr of evolution. Second, a sum of net viscous and gravitational torques is always *negative*. This fact constitutes a fundamental property of self-gravitating circumstellar discs, both viscous and non-viscous. The net negative torque is related to the ongoing accretion of gas on to a protostar – the accreted material removes the disc angular momentum, which may be later ejected to the external environment via magnetic braking and protostellar jets. As a consequence, the rate of change of the disc angular momentum and the net torque are both negative. It is also interesting to note that the net viscous torque in the first 10^5 yr of evolution is positive. This is related to the fact that most of the disc in this phase is characterized by the dynamic viscosity that declines with radius faster than $r^{-0.5}$. Indeed, it can be shown that an axisymmetric Keplerian disc has a positive viscous torque, i.e. $r(\nabla \cdot \Pi)_\phi > 0$ if $\mu \propto r^\beta$, where $\beta < -0.5$.

3.3 Accretion rates and disc masses

Figure 5 demonstrates that circumstellar discs evolve through two distinct physical regimes during their long-term evolution, gravity-dominated and viscosity-dominated. The former always precedes the latter and the time when the viscosity-dominated regime takes over, or even its existence, depends on the value of α . In each of the two regimes, radial transport of mass and angular momentum is controlled by principally different mechanisms and the mass accretion rates on to the central star should bear the imprints of these differences.

The right column in Fig. 6 shows (from top to bottom) the mass accretion rate in model 1 ($\alpha = 0$), model 3 ($\alpha = 10^{-3}$), model 4 ($\alpha = 10^{-2}$), and model 5 ($\alpha = 10^{-1}$) as a function of time. The mass accretion rate is computed as $\dot{M} = -2\pi r v_r \Sigma(r)$, where v_r is the radial velocity at the inner inflow boundary $r = 5$ AU. In all four models the evolution starts with a sharp rise of \dot{M} to a maximum value, manifesting the formation of a central star at $t \approx 0.06$ Myr, and continues with a short phase of near constant accretion, in which matter is directly accreted on to the star. The disc forms at $t \approx 0.14$ Myr and the subsequent accretion history is considerably different between the models. The non-viscous model 1 develops short-lived mass accretion bursts⁴ with $\dot{M} \geq 10^{-4} M_\odot \text{ yr}^{-1}$, while the quiescent phase is characterized by a much lower accretion rate in the range a few $\times 10^{-7} - 10^{-8} M_\odot \text{ yr}^{-1}$. On the other hand, the $\alpha = 10^{-1}$ model 5 shows virtually no bursts, while the $\alpha = 10^{-2}$ model 4 has only a few of them. It is evident that the burst activity diminishes along a sequence of increasing α . There is *no* quiescent phase of low-rate accretion in models 4 and 5 – the mass accretion rate gradually declines with time from a few $\times 10^{-6} M_\odot \text{ yr}^{-1}$ just after the disc formation to $10^{-8} M_\odot \text{ yr}^{-1}$ (and lower) at 2.0 Myr.

There are two observationally valuable consequences of the burst phenomenon. First, it can provide an explanation for the FU Orionis variables. The apparent lack of bursts in the viscous discs will make it more difficult to account for the burst activity, though other burst mechanisms may be operational in the inner disc at $r \lesssim 1$ AU (e.g. Bell & Lin 1991). Second, the existence of the quiescent phase of accretion in the *early* evolutionary phase can potentially be linked with a recent detection of Very Low Luminosity Objects (VeLLOs) by the *Spitzer Space Telescope* (e.g. Young et al. 2004). A previously detected object in this category is IRAM 04191 (André et al. 1999); for another example see Stecklum et al. (2007). All of these are objects with luminosity $L \leq 0.1 L_\odot$ embedded within dense cores, which, based on previous observations, were often classified as starless. Their association with dense cores and their low luminosity suggests that they are *young* objects that feature some combination of a sub-solar mass and low accretion rate. They might be proto-brown dwarfs, but Fig. 6 offers an alternative. The non-viscous model 1 can account for VeLLOs as young protostars in the quiescent accretion phase with $\dot{M} \sim 10^{-8} M_\odot \text{ yr}^{-1}$,

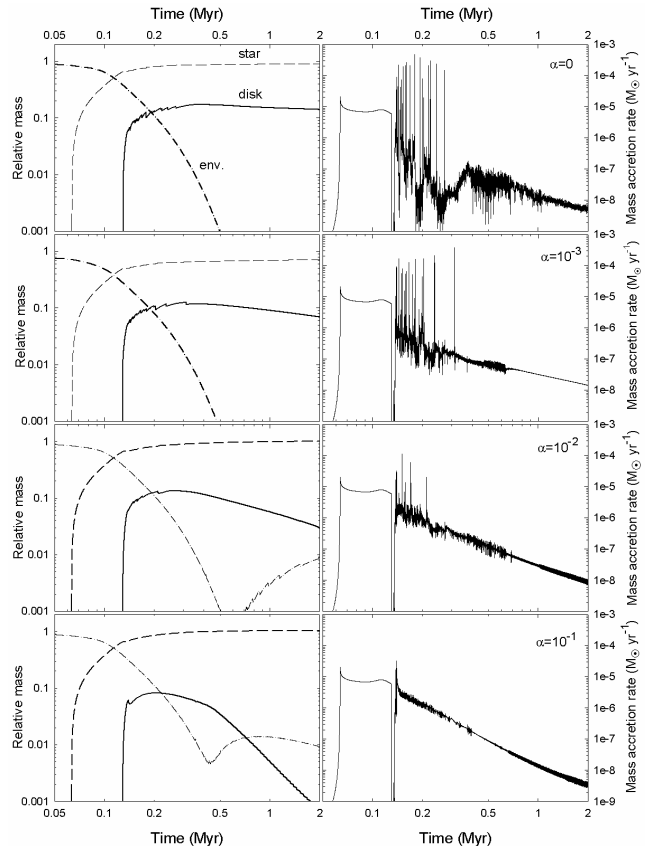


Figure 6. Right column: temporal evolution of the mass accretion rate \dot{M} in the $\alpha = 0$ model 1 (top), $\alpha = 10^{-2}$ model 4 (middle), and $\alpha = 10^{-1}$ model 5 (bottom). Left column: temporal evolution of the disc mass (solid lines), stellar mass (dashed lines), and envelope mass (dot-dashed lines) in model 1 (top), model 4 (middle), and model 5 (bottom). All masses are relative to the initial cloud mass $M_{\text{cl}} = 0.8 M_\odot$.

which for the protostellar mass of $\sim 1.0 M_\odot$ would correspond to the accretion luminosity 3% that of the solar. Clearly, the viscous models 4 and 5 cannot account for VeLLOs, as their mass accretion rates in the early disc evolution are too high. The identity of these objects can ultimately be revealed by studying the chemical evolution of brown dwarfs and young protostars (Lee 2007).

Distinct changes in the radial structure of circumstellar discs along the sequence of increasing α , as seen in Figs 1-4, suggest that viscosity and gravity-dominated discs may have quite different masses. The left column in Fig. 6 shows disc masses (solid lines), stellar masses (dashed lines) and envelope masses (dot-dashed lines), all relative to the initial cloud core mass $M_{\text{cl}} = 0.8 M_\odot$, in (from top to bottom) model 1, model 3, model 4, and model 5. In the $\alpha = 0$ model 1 the relative disc mass reaches a maximum value of 14% soon after the disc formation and is not significantly changing afterwards. On the contrary, disc masses in the $\alpha = 10^{-2}$ models 4 and $\alpha = 10^{-1}$ model 5, though attaining similar maximum values soon after the disc formation, show a significant decline with time in the subsequent evolution. In particular, the disc mass in model 4 drops to only 3% that of the central star at 2 Myr, while the disc in model 5 is virtually depleted after 2 Myr of evolution. At a first glance,

⁴ The burst phenomenon is caused by disc fragmentation due to high rates of mass infall from the envelope in the early embedded phase and is described in detail in Vorobyov & Basu (2005, 2006). A highly variable accretion was also reported in the case of isolated massive discs by Lodato & Rice (2005).

it may seem surprising that viscous and non-viscous models have similar (within a factor of 2) disc masses in the early evolution although the mass accretion rates in the viscous models appear (by eye) to be greater than those in the non-viscous model. This paradox is resolved by the fact that the bursts are very efficient in regulating the disc mass. During each burst a significant amount of mass ($0.01 - 0.05 M_{\odot}$) is accreted on to the protostar (Vorobyov & Basu 2005, 2006).

A decline in the disc mass in models 4 and 5 seen in the late evolution is caused not only by accretion on to the central star but also by disc expansion due to viscous torques. The dot-dashed lines in Fig. 6 illustrate this phenomenon – the envelopes in models 4 and 5 are not completely depleted by the end of numerical simulations (as in model 1 and 3) but appear to gain some mass in the late evolution. This mass is coming from the disc, which dilutes and expands in the late evolution (see Figs 3 and 4), thus losing part of its material to the external environment. The disc expansion is explained by the fact that μ in the outer disc scales as r^{β} , where $\beta < -0.5$, which causes the disc material to be transported outward

Figure 6 demonstrates an important ingredient of our numerical model – our discs are formed self-consistently during numerical simulation and not introduced in the beginning of numerical simulations. Indeed, the time evolution of the mass accretion rate (MAR) in Fig. 6 can be split into three phases. In the first phase, the MAR is characterized by a sharp growth from a negligible value to a peak value of approximately $2 \times 10^{-5} M_{\odot} \text{ yr}^{-1}$. This behaviour is characteristic for the runaway collapse phase and stellar core formation phase in spherically symmetric cloud core collapse simulations (e.g. Foster & Chevalier 1993; Vorobyov & Basu 2005). The second phase is characterized by a near-constant MAR at approximately $10^{-5} M_{\odot} \text{ yr}^{-1}$. This is typical for collapsing self-similar spherically symmetric cloud cores (e.g. Shu 1977). In these two early phases, the infalling envelope accretes directly onto the central star. At approximately 0.14 Myr a first infalling layer of gas hits the centrifugal barrier at $r = 5$ AU and a centrifugally balanced disc begins to form⁵. Since then, the system enters a qualitatively distinct phase of disc accretion. Because the forming disc is too small and in the state of near centrifugal balance, the MAR drops by many orders of magnitude. This sharp drop is a signature of the disc formation and cannot be present in numerical simulations if they start right from the disc phase. Soon after the disc has formed, it accumulates enough mass to trigger radial mass transport and the subsequent time behaviour of the MAR is controlled by the interplay of self-gravity and viscosity.

4 STIFFER EQUATION OF STATE

Numerical simulations with a more realistic treatment of the energy balance indicate that the strength of gravitational instability in general and the disc propensity to fragmentation in particular depend on the characteristic time of disc cooling and, hence, on the disc temperature (e.g. Gammie 2001;

⁵ In reality, the disc forms earlier but we cannot resolve its evolution within the inner 5 AU due to the use of the sink cell

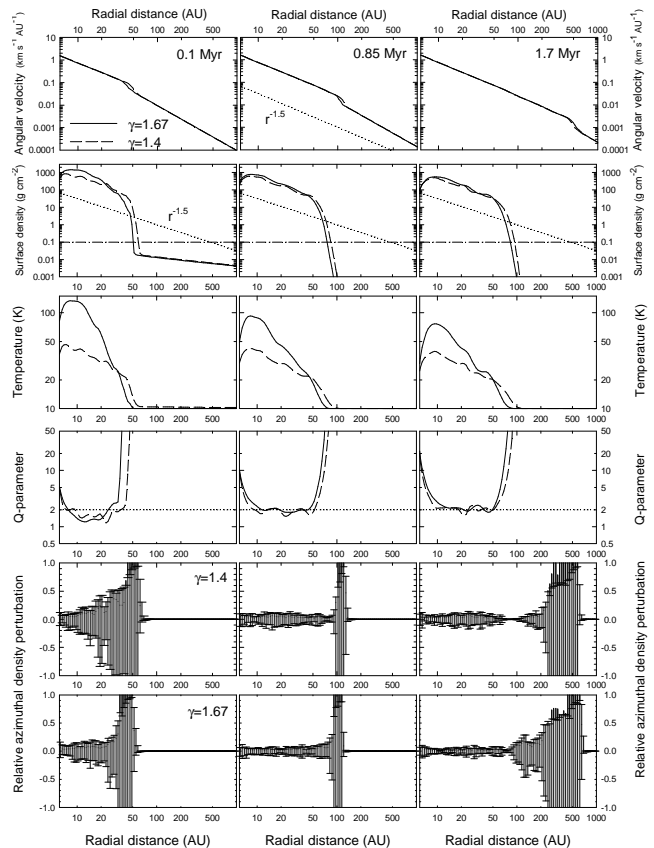


Figure 7. Radial structure of a purely self-gravitating disc ($\alpha = 0$) in the $\gamma = 1.4$ model (dashed lines) and $\gamma = 1.67$ model (solid lines). The disc age is indicated in the top frame of each column. See captions to Fig. 1 for details.

Johnson & Gammie 2003; Rice et al. 2003; Lodato & Rice 2004; Meĵia et al. 2005). In this section we consider the effect of increasing the ratio of specific heats from $\gamma = 1.4$ to $\gamma = 1.67$ in a purely self-gravitating disc. This stiffening of the barotropic equation of state should raise disc temperatures and mimic the effect of a longer characteristic cooling time.

In Fig. 7 we compare the disc radial structure in models with $\gamma = 1.4$ (dashed lines) and $\gamma = 1.67$ (solid lines). It is evident that an increase in γ results in a factor of two higher gas temperatures in the disc, especially in its inner region. At the same time, the gas surface density also increases and the resulting Toomre Q -parameter changes insignificantly and (in some parts of the disc) may even drop below the values characteristic for the colder disc. The radial distribution of the gas surface density scales as $r^{-1.5}$ throughout most of the evolution, except for the very early phase when $\Sigma \propto r^{-2.0}$. The relative azimuthal density perturbations are slightly smaller than those in the colder disc. To summarize, the most substantial change is seen in the radial gas temperature distribution. However, since the sound speed is proportional to the square root of the gas temperature and the gas surface density also increases, the resulting Toomre parameter does not change significantly.

Our next step is to compare the mass accretion rates in models with different values of γ . The top and bottom panels in Fig. 8 show \dot{M} in models with $\gamma = 1.4$ and $\gamma = 1.67$, re-

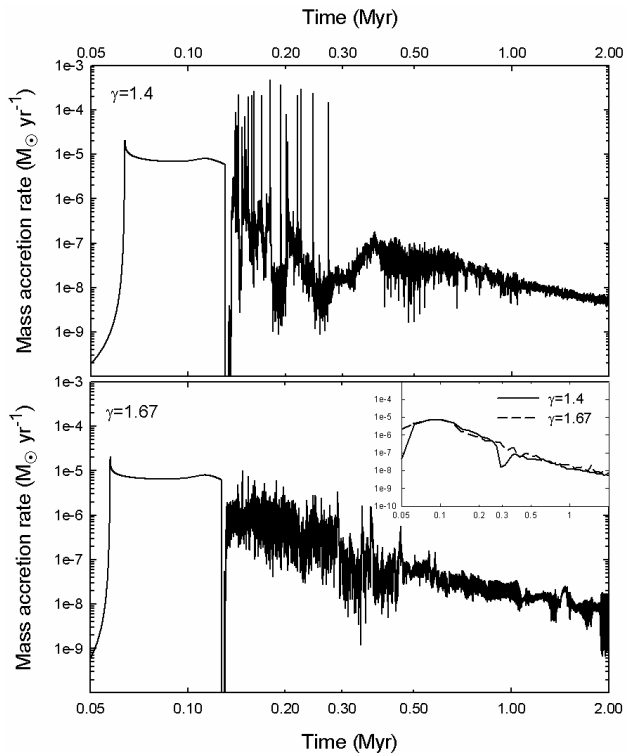


Figure 8. Mass accretion rates in the $\gamma = 1.4$ model (top) and $\gamma = 1.67$ model (bottom) as a function of time. The both models are non-viscous ($\alpha = 0$). The insert shows the rates averaged over a period of 2×10^4 yr in the $\gamma = 1.4$ model (dashed line) and $\gamma = 1.67$ model (solid line).

spectively. A visual inspection of the figure reveals that the most noticeable change in the time behaviour of \dot{M} occurs in the early phase of disc evolution between 0.14 Myr and 0.4 Myr. While the $\gamma = 1.4$ disc exhibits extremely varying rates with short bursts followed by longer periods of quiescent accretion, the $\gamma = 1.67$ disc shows a gradually declining accretion rate with an order of magnitude fluctuations or flickering around mean values. However, the time-averaged (over 2×10^4 Myr) mass accretion rates are not too dissimilar, as is seen in the insert to Fig. 7. More specifically, the $\gamma = 1.4$ disc is characterized by slightly larger/smaller accretion in the early/late phase than the $\gamma = 1.67$ disc. It is worth mentioning that this tendency is also seen when shorter characteristic cooling times are considered. For instance, the $\gamma = 1.2$ disc⁶ has slightly larger/smaller accretion in the early/late phase than the $\gamma = 1.4$ disc. In any case, accretion rates show only a factor of unity difference.

Why are the time-averaged mass accretion rates rather similar in both models? At a first glance, one might expect a much large contrast, since an increase in gas temperature is expected to moderate gravitational instability and reduce accretion triggered by gravitational torques. However, as was noticed by Cai et al. (2008), a moderate increase in disc temperature may in fact promote accretion due to the growing relative strength of lower order spiral modes in the

disc. The global nature of lower order modes makes them more efficient agents for the radial mass transport in the disc than higher order modes, the latter tend to produce more fluctuations and cancellation in the net gravitational torque.

In order to visualize this effect and the strength of spiral modes in the disc, we compute the global Fourier amplitudes (GFA) defined as

$$C_m(t) = \frac{1}{M_d} \left| \int_0^{2\pi} \int_{r_{\text{in}}}^{r_{\text{disc}}} \Sigma(r, \phi, t) e^{im\phi} r dr d\phi \right|, \quad (10)$$

where M_d is the disc mass and r_{disc} is the disc's physical outer radius. The instantaneous GFA show considerable fluctuations and we have to time average them over 2×10^4 yr in order to produce a smooth output. The temporal evolution of the time-averaged GFA (log units) for the $\gamma = 1.4$ (top) and $\gamma = 1.67$ (bottom) models is shown in the left column of Fig. 9. The time behaviour of the GFA is indicative of two qualitatively different phases in the disc evolution. In the early phase ($t \lesssim 0.6$ Myr), a clear segregation between the modes is evident – the lower order mode dominates its immediate higher order neighbour in both models. In particular, the $m = 1$ mode is almost always the strongest one. The modes also show a clear tendency to decrease in magnitude with time, which explains a gradual decline in the time-averaged mass accretion rates shown in the insert of Fig. 8. The GFA of the $\gamma = 1.4$ disc are somewhat larger than those of the $\gamma = 1.67$ disc, except probably for $C_1(t)$, indicating that gravitational instability is stronger in the $\gamma = 1.4$ disc. The same effect is also seen when we compare the $\gamma = 1.2$ and $\gamma = 1.4$ discs – the former has larger GFA than the latter. In the late phase, however, this clear picture breaks into a kaleidoscope of modes, with higher order modes $m \geq 2$ competing for dominance with each other and the $m = 1$ mode being almost always the weakest one. The GFA have dropped in magnitude considerably. However, accretion on to the star does not terminate since the effect of these mode fluctuations is to produce a net *negative* torque in the inner disc (Vorobyov & Basu 2007). These mode fluctuations are not a numerical noise but are rather caused by ongoing low-amplitude non-axisymmetric density perturbations sustained by swing amplification at the disc's sharp outer edge. As was shown by Vorobyov & Basu (2007), self-gravity of the disc is essential for these density perturbations to persist into the late disc evolution. The density perturbations (and associated accretion) quickly disappear if self-gravity is switched off.

In the right column of Fig. 9 we plot the ratios C_m/C_1 as a function of time for the $\gamma = 1.4$ disc (top) and $\gamma = 1.67$ disc (bottom). It is evident that the relative input from the $m \geq 2$ modes is larger in the $\gamma = 1.4$ disc than in the $\gamma = 1.67$ one. This implies that the mode-to-mode interaction may produce more cancellation in the net gravitational torque in the colder $\gamma = 1.4$ disc than in the hotter $\gamma = 1.67$ disc. As a result, the efficiency of mass transport (due to all modes) reduces in the colder disc and becomes similar to that of the hotter disc, even though most of the GFA are in fact larger in the former than in the latter. This may seem counterintuitive but the same effect was found in numerical simulations of envelope-irradiated discs by Cai et al. (2008). It is worth mentioning that a similar modal behaviour was found when $\gamma = 1.2$ and $\gamma = 1.4$ discs are compared in our numerical

⁶ It is problematic to consider values of γ smaller than $\gamma = 1.2$, since equation (5) tends to overestimate gas pressure when $\gamma \rightarrow 1.0$.

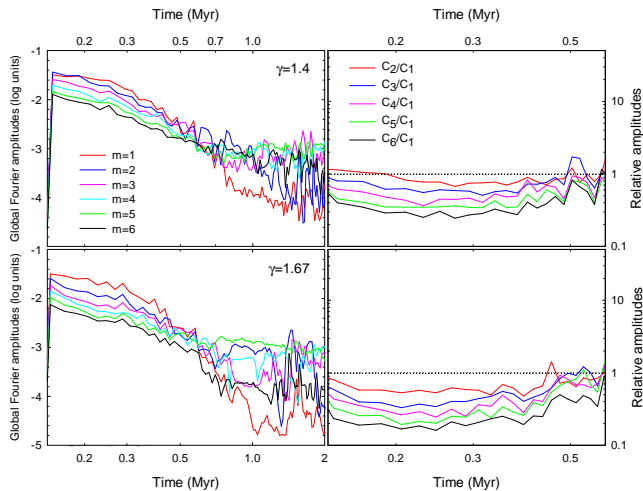


Figure 9. **Left:** Global Fourier amplitudes C_m (in log units) for modes $m = 1 - 6$ as a function of time in the $\gamma = 1.4$ disc (top) and $\gamma = 1.67$ disc (bottom). **Right:** Ratio C_m/C_1 of the higher order modes $m \geq 2$ to the lowest order $m = 1$ mode for the $\gamma = 1.4$ disc (top) and $\gamma = 1.67$ disc (bottom).

simulations – the relative input from the $m \geq 2$ modes is larger in the $\gamma = 1.2$ disc than in the $\gamma = 1.4$ one. The effect is not large but is certainly noticeable.

Alternatively, the similarity of mass accretion rates in discs characterized by different γ may be merely a result of the self-regulating nature of embedded accretion discs, which re-adjust their gravitational torques (e.g. by increasing/decreasing surface densities, temperatures, etc.) in order to pass on the mass flux coming from the envelope.

Figure 10 shows the temporal evolution of viscous and gravitational net torques for the same models as in Fig. 5 but with $\gamma = 1.67$. The comparison of Figs 5 and 10 indicates that the time behaviour of the torques in both figures is quite similar. There is a slight increase in the strength of the viscous torques in models with $\gamma = 1.67$ caused by a higher (on averaged) disc temperature than in models with $\gamma = 1.4$. In particular, the very early evolution of the $\alpha = 0.1$ model ($t \leq 0.02$ Myr) is dominated by viscosity, while in the corresponding model with $\gamma = 1.4$ both the viscous and gravitational torques are nearly equal. We conclude that a (modest) increase in disc temperature does not noticeably affect the disc accretion properties averaged over many orbital periods ($\sim 10^4$ yr) but can substantially change the instantaneous accretion rates. We also note that although the $\gamma = 1.67$ disc does not show vigorous bursts of mass accretion (but rather an order of magnitude flickering around mean values), the bursts can be re-established by increasing the initial rotation velocity of the cloud core (e.g. Vorobyov & Basu 2006).

5 DISCUSSION

5.1 Constraints on turbulent viscosity

There are several known physical processes that can contribute to the radial transport of mass and angular momentum in circumstellar discs. These transport mechanisms include gravitational torques, either due to internal (self-gravity) or external (companion star) sources, and turbu-

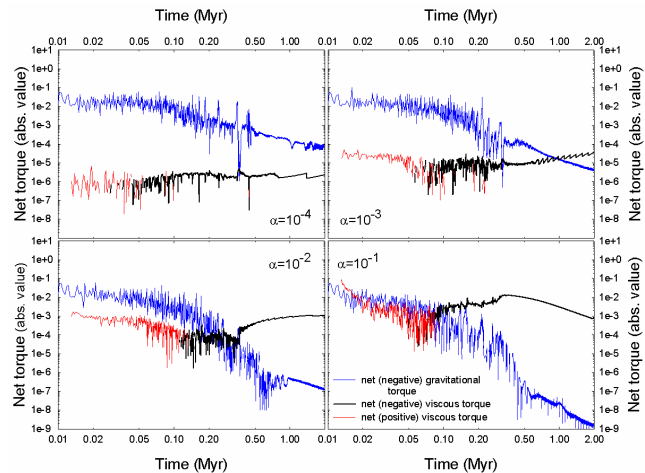


Figure 10. The same as Fig. 5 only for models with $\gamma = 1.67$.

lent viscosity. The effect of self-gravity on the secular evolution of a circumstellar disc has been considered in our previous paper (Vorobyov & Basu 2007). In this paper we added the effect of turbulent viscosity due to yet unspecified source of turbulence. Physical processes in circumstellar discs that can, under specific conditions, give rise to turbulence include the magneto-rotational instability and vertical convection. The latter may be heavily suppressed in the externally heated discs (Ruden & Pollack 1991), which leaves the MRI as the most probable source of turbulence in circumstellar discs. Afshordi et al. (2005) have recently argued on analytical grounds that hydrodynamic turbulence (not related to the MRI) can arise in cold Keplerian discs characterized by Reynolds numbers $\gtrsim 10^4$ and having both the fine-tuned conditions and appropriate feedback mechanism, though this idea has not been proven so far by numerical simulations.

Many numerical efforts to characterize the MRI-induced turbulent viscosity qualitatively have been made in the recent years. These include local shearing box models (e.g. Brandenburg et al. 1996; Stone et al. 1996; Fleming & Stone 2003; Sato et al. 2004) and global magnetohydrodynamic simulations of accretion discs (e.g. Armitage 1998), though the latter are usually limited by a small number of orbital periods. Most authors calculate the mean ratios of the Maxwell and Reynolds stresses versus midplane gas pressure, $T_{r\phi}^B/P_0$ and $T_{r\phi}^{Re}/P_0$, respectively, which, to a factor of unity, are proportional to α in Keplerian discs⁷.

The derived values of α vary significantly between the studies. For instance, Hartmann et al. (1998) derived $\alpha \approx 0.01$ using observed disc sizes and a simple model for the evolution of an axisymmetric viscous disc, in which viscosity is a power-law function of radius. Fleming & Stone (2003) have employed a stratified model of accretion discs in a shearing box approximation, in which the upper layers are MRI-active while the central regions are quiescent. They found

⁷ In fact, this is true only for axisymmetric discs, in which $T_{r\phi}^B = (d \log \Omega / d \log r) \alpha P_0$ and the rate of strain $d \log \Omega / d \log r$ is constant (e.g. $-3/2$ in Keplerian discs). In non-axisymmetric discs the relation between $T_{r\phi}^B$ and P_0 is more complex.

that T_{xy}^B/P_0 has a mean value of about 10^{-3} in the MRI-active upper layers but drops to a negligible value in the midplane. On the other hand, T_{xy}^{Re}/P_0 in the vertical direction is roughly constant at a few $\times 10^{-4}$. This implies mean values of α in the range $10^{-4} - 10^{-3}$. Low mean values of α were also reported by Brandenburg et al. ($\alpha = 0.007$) and Stone et al. ($\alpha \lesssim 0.01$). On the other hand, global numerical simulations tend to yield larger values for α . For instance, Armitage (1998) found mean values between 0.05 and 0.1.

Large variations in α , both in space and time, imply that the development of the magneto-rotational instability is strongly dependent on the local conditions in the disc. Nevertheless, we can still learn about circumstellar discs from a simple model used in our paper, if we assume that the constant α represents a mean value, time-averaged over many orbital periods of the disc. Radial variations in α may (and should) be present in the disc but it requires a more thorough consideration of the disc physics (i.e. the ionization balance) and is left for a follow-up paper.

Our numerical simulations unambiguously demonstrate that circumstellar discs cannot sustain turbulent viscosity with a spatially and temporally averaged $\alpha \gtrsim 0.1$. Such discs would have vanished during just one million year of evolution. The ubiquitous presence of older discs makes such large values of α unlikely. On the other hand, low values of α of order 10^{-4} make little effect on the secular disc evolution, which in this case is completely governed by gravitational torques rather than viscous ones. In the case of $\alpha = 10^{-3}$, viscosity does have some effect on the disc radial structure but the magnitude of these changes are modest – the surface density profile becomes somewhat shallower in the inner disc and at the disc’s outer boundary, and the disc size increases by a factor of 2 as compared to that of the non-viscous one. The $\alpha = 0.01$ disc sees considerable changes in its radial structure in the late evolution, and the gravitational stabilization of such discs presents difficulty to account for non-axisymmetric structure and poses problems for the theoretical idea of giant planet formation via direct gravitational instability. Moreover, the gas surface density in the entire $\alpha = 0.01$ disc becomes lower than that of the MMSN after 1.0 Myr. This also poses problems for planet formation models, which often require discs with gas surface densities a few times greater than that of the MMSN (e.g. Ida & Lin 2004). We conclude that the mean value of α (averaged over many orbital periods) should lie in the range $10^{-3} - 10^{-2}$, although large transient variations around these values can still be present in real discs.

5.2 Effective viscosity due to gravitational torques

An interesting way to account for the *combined* effect of gravitational and viscous torques is to calculate an ‘effective alpha’ α_{eff} near the inner boundary of our simulation⁸. If we apply the steady-state mass accretion rate formula for thin viscous discs and also apply the α -prescription, then

$$\dot{M} = 3\pi\nu\Sigma = 3\pi\alpha_{\text{eff}}\tilde{c}_s Z\Sigma. \quad (11)$$

We calculate \dot{M} in each simulation at the boundary of the sink cell ($r = 5$ AU), and \tilde{c}_s , Z , and Σ at some distance

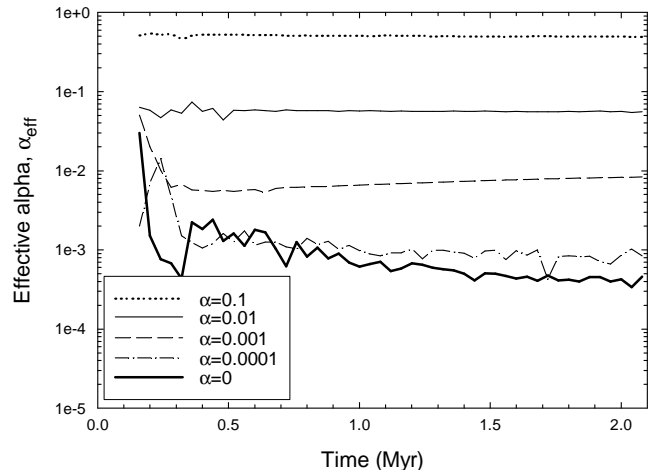


Figure 11. Temporal evolution of the effective viscosity parameter α_{eff} that accounts for both viscous and gravitational torques, for each of our models.

($r \approx 9$ AU) since Σ decreases somewhat near the sink cell. These numbers are used to generate α_{eff} , which is plotted versus time in Fig. 11 for each of our models. The values of α_{eff} may be scaled down by a factor ≈ 2 if use also the values of \dot{M} at 9 AU instead of 5 AU. Clearly, gravitational torques in the absence of turbulent viscosity accounts for an α_{eff} in the range $10^{-4} - 10^{-3}$ during the late evolution. This is why the addition of a viscous α of at least 10^{-3} is required to see significant changes in the disc evolution.

It is also interesting to compare our results with previous numerical simulations of the secular evolution of viscous circumstellar discs. For instance, Lin & Pringle (1990) have considered the formation and evolution of a circumstellar disc formed during the collapse of a rotating cloud core with initial mass $1.0 M_{\odot}$. They use the usual diffusion equation describing the evolution of the surface density in a viscous *axisymmetric* accretion disc (Lynden-Bell & Pringle 1974)

$$\frac{\partial \Sigma}{\partial t} = -\frac{1}{r} \frac{\partial}{\partial r} \left[\frac{1}{(r^2 \Omega)'} \frac{\partial}{\partial r} (\nu \Sigma r^3 \Omega') \right], \quad (12)$$

complemented by some form of the energy equation describing the internal energy balance in the disc due to viscous heating, energy input from the accretion process, and disc radiative cooling. Our model, though neglecting detailed thermodynamics, accounts for a possible disc asymmetry by directly solving the corresponding fluid dynamics equations for a thin disc. The effective kinematic viscosity in Lin & Pringle’s model comes from turbulent viscosity and gravitational instability, the former is parameterized using a usual Shakura & Sunyaev α -prescription (eq. 1), while the latter is taken into account following Lin & Pringle (1987):

$$\nu_{\text{g}} = \begin{cases} \frac{2\mu}{3} \left(\frac{Q^2}{Q^2} - 1 \right) \left(\frac{c^2}{\Omega} \right) & \text{if } Q \leq Q_c \\ 0 & \text{otherwise.} \end{cases} \quad (13)$$

We need to parameterize only the viscous torques, the effect of gravitational torques is taken into account self-consistently.

Both approaches yield circumstellar discs that share some common characteristics. For instance, Lin & Pringle’s model A1 ($\alpha, \mu = 0.01$) produces a rather cold disc ($T \sim$

⁸ For various methods to define α_{eff} see e.g. Lodato (2007)

10 K) that features a near-flat surface density profile near the inner boundary and scales roughly as r^{-1} at 100 – 1000 AU. Their disc has a sharp outer edge upon formation but it spreads out in the course of evolution. These features are also seen in our modeling, though our disc in the corresponding model 3 has a smaller size (~ 300 AU) and a lower surface density. This brings about the most striking difference found between the two approaches – the derived disc masses. Lin & Pringle (1990) have reported disc masses that are an order of magnitude larger than the corresponding stellar masses in the early evolution. Although this large difference reduces with time, the disc mass is still comparable to that of the star in the late evolution ($t \gtrsim 1.0$ Myr), irrespective of the value of α . Such massive discs are not observed. Our models predict maximum disc-to-star mass ratios of $\xi = 14\%$ (model 1), and this value quickly reduces with time for the viscosity-dominated discs (e.g. model 3). Although our obtained values of ξ for non-viscous models still seem to be greater than those usually inferred for T Tauri stars, 0.5%–1% (e.g. Andrews & Williams 2005), they are not unfeasible given that the measured disc masses may be underestimated by conventional methods by as much as an order of magnitude (e.g. Hartmann et al. 2006). Figure 5 indicates that gravitational torques are a dominant mechanism of mass and angular momentum transport in the disc in its early evolutionary phase.

The fact that Lin & Pringle (1990) obtain overmassive discs in their numerical simulations suggests that either the parameterization given by equation (13) is inadequate, certainly in the early disc evolution, or the ratio of rotational-to-gravitational energies β in their model is too large, resulting in most of the initial cloud mass landing on to the disc and through the disc on to the star rather than directly on to the star. In other words, the phase of near constant accretion of matter from the envelope directly on to the star (see Fig. 6) is very short in the Lin & Pringle model and the disc is not capable of processing the infalling mass to the star fast enough to keep its mass low. Indeed, Lin & Pringle have adopted β in the range 0.25 – 0.64, which is much larger than the values recently inferred for molecular cloud cores by Caselli et al. (2002), $\beta = 10^{-4} - 0.07$. In our model, β is set to 1.4×10^{-3} .

6 SUMMARY

Using numerical hydrodynamics simulations we have studied the long-term evolution (2.0 Myr) of self-consistently formed, self-gravitating circumstellar discs that are subject to turbulent viscosity. We seek to determine the effect of viscosity on the radial structure and accretion properties of self-gravitating discs around low-mass ($\sim 0.7 M_{\odot}$) protostars. We make no specific assumptions about the source of turbulence in circumstellar discs and parameterize the magnitude of turbulent viscosity using the usual α -prescription (Shakura & Sunyaev 1973). Four models with a spatially and temporally uniform values of $\alpha = 10^{-4}$, 10^{-3} , 10^{-2} , and 10^{-1} were considered and compared with the standard model characterized by $\alpha = 0$. We find the following.

(i) Low values of α of order 10^{-4} make little effect on the secular evolution of a self-gravitating disc, the radial structure and accretion properties of which in this case are

completely determined by gravitational torques rather than by viscous ones.

(ii) At values α of order 10^{-2} , the discs see considerable changes in their radial structure, with a surface density that is axisymmetric and has values that are already below that of the MMSN by 1 Myr. This is problematical for planet formation.

(iii) High values of α of order 10^{-1} make a catastrophic effect on the disc secular evolution. Most of the disc mass is quickly accreted on to the protostar and the rest is dispersed to the external environment. The disc mean surface density drops below 1.0 g cm^{-2} during just 1 – 2 Myr.

(iv) The net viscous torque in the disc is *positive* in the early evolution ($\lesssim 0.1$ Myr) and negative afterwards. On the other hand, the total (viscous plus gravitational) net torque is always negative, which is related to the removal of angular momentum from the disc by gas that is accreted in to the central region.

(v) Use of a stiffer barotropic equation of state ($\gamma = 1.67$ instead of $\gamma = 1.4$) and associated rise in disc temperature can substantially affect the instantaneous accretion rates (particularly in the early evolution) but have little effect on the disc accretion properties averaged over many disc orbital periods ($\sim 10^4$ yr). This is because a decrease in the intensity of mass accretion bursts in the hotter disc is compensated by an increase in the relative strength of lower order spiral modes ($m \leq 2$), which are the most efficient agents for radial mass transport in the disc.

(vi) Viscous-dominated models have difficulty to account for some physical properties of circumstellar discs. For instance, they become virtually axisymmetric and gravitationally stable after just 1.0 Myr of evolution. Moreover, the lack of a quiescent phase of low-rate mass accretion ($\dot{M} \sim 10^{-8} M_{\odot} \text{ yr}^{-1}$) in the early evolution of viscous discs will make it difficult to account for Very Low Luminosity Objects (VeLLOs), which are presumably young objects that feature some combination of a sub-solar mass and low accretion rate (Young et al. 2004; André et al. 1999; Stecklum et al. 2007). On the other hand, non-viscous self-gravitating models can naturally account for both the apparent disc non-axisymmetry and a phase of very low luminosity.

We emphasize that the α -parameter in our models does not include a (possible) contribution from Reynolds stresses due to self-gravity. This fact should be taken into account when comparing our predicted values of α with those derived in other studies, which may include a contribution from the gravitational Reynolds stresses (e.g. Gammie 2001). We have also not considered a possible contribution of Reynolds stresses in the transport of mass and angular momentum. According to Lodato & Rice (2004), this contribution may be comparable to that of the gravitational torques, which means that the importance of self-gravity may be underestimated by a factor of 2.

ACKNOWLEDGMENTS

We are thankful to the referee, Giuseppe Lodato, for the insightful comments that helped improve the manuscript. E.I.V. gratefully acknowledges present support from an ACEnet Fellowship. SB was supported by a grant from

the Natural Sciences and Engineering Research Council of Canada. Numerical simulations were done on the Atlantic Computational Excellence Network (ACEnet) and Shared Hierarchical Academic Research Computing Network (SHARCNET).

APPENDIX A: DISC SCALE HEIGHT

We derive the disc vertical scale height Z at each computational cell via the equation of local vertical pressure balance

$$\rho \tilde{c}_s^2 = 2 \int_0^Z \rho (g_{z,\text{gas}} + g_{z,\text{st}}) dz, \quad (\text{A1})$$

where ρ is the gas volume density, $g_{z,\text{gas}}$ and $g_{z,\text{st}}$ are the vertical gravitational accelerations due to self-gravity of a gas layer and gravitational pull of a central star, respectively. Assuming that ρ is a slowly varying function of vertical distance z between $z = 0$ (midplane) and $z = Z$ (i.e. $\Sigma = 2 Z \rho$) and using the Gauss theorem, one can show that

$$\int_0^Z \rho g_{z,\text{gas}} dz = \frac{\pi}{4} G \Sigma^2, \quad (\text{A2})$$

$$\int_0^Z \rho g_{z,\text{st}} dz = \frac{GM_* \rho}{r} \left\{ 1 - \left[1 + \left(\frac{\Sigma}{2\rho r} \right) \right]^{-1/2} \right\} \quad (\text{A3})$$

where r is the radial distance and M_* is the mass of the central star. Substituting equations (A2) and (A3) back into equation (A1) we obtain

$$\rho \tilde{c}_s^2 = \frac{\pi}{2} G \Sigma^2 + \frac{2GM_* \rho}{r} \left\{ 1 - \left[1 + \left(\frac{\Sigma}{2\rho r} \right) \right]^{-1/2} \right\}. \quad (\text{A4})$$

This can be solved for ρ given the model's known \tilde{c}_s^2 , Σ , and M_* , using Newton-Raphson iteration. The vertical scale height is finally derived as $Z = \Sigma/(2\rho)$.

APPENDIX B: DIVERGENCE OF THE VISCOUS STRESS TENSOR

The components of $\nabla \cdot \mathbf{\Pi}$ in polar coordinates (r, ϕ) are

$$(\nabla \cdot \mathbf{\Pi})_r = \frac{1}{r} \frac{\partial}{\partial r} r \Pi_{rr} + \frac{1}{r} \frac{\partial}{\partial \phi} \Pi_{r\phi} - \frac{\Pi_{\phi\phi}}{r}, \quad (\text{B1})$$

$$(\nabla \cdot \mathbf{\Pi})_\phi = \frac{\partial}{\partial r} \Pi_{r\phi} + \frac{1}{r} \frac{\partial}{\partial \phi} \Pi_{\phi\phi} + 2 \frac{\Pi_{r\phi}}{r}, \quad (\text{B2})$$

where we have neglected the contribution from off-diagonal components Π_{rz} and $\Pi_{\phi z}$.

REFERENCES

Afshordi, N., Mukhopadhyay, B., Narayan, R., 2005, ApJ, 629, 373
 André, P., Motte, F., Bacmann, A., 1999, ApJ, 513, L57
 Andrews, S. M., Williams, J. P., 2005, ApJ, 631, 1134
 Armitage, P. J., 1998, ApJ, 501, L189
 Balbus, S. A., Hawley, J. F., 1991, ApJ, 376, 214
 Basu S., 1997, ApJ, 485, 240
 Bell, K. R., Lin, D. N. C., 1994, ApJ, 427, 987
 Boss, A. 2008, ApJ, 677, 607

Brandenburg, A., Nordlund, A., Stein, R. F., Torkelsson, U., 1996, ApJ, 458, L45
 Cai, K., Durisen, R. H., Boley, A. C., Pickett, M. K., Mejía, A. C. 2008, ApJ, 673, 1138
 Caselli, P., Benson, P. J., Myers, P. C., Tafalla, M., 2002, ApJ, 572, 238
 Fleming, T., Stone, J. M., 2003, ApJ, 585, 908
 Foster, P. N., Chevalier, R. A., 1993, ApJ, 416, 303
 Fromang, S., Balbus, S. A., De Villiers, J.-P., 2004, ApJ, 616, 357
 Fromang, S., Balbus, S. A., Terquem, C., De Villiers, J.-P., 2004, ApJ, 616, 364
 Fukagawa, M., et al., 2004, ApJ, 605, L53
 Gammie, C. F., 2001, ApJ, 553, 174
 Grady, C. A., et al., 2001, AJ, 122, 3396
 Hartmann, L., Calvet, N., Gullbring, E., D'Alessio, P., 1998, ApJ, 495, 385
 Hartmann, L., D'Alessio, P., Calvet, N., & Muzerolle, J., 2006, ApJ, 648, 484
 Hawley, J. F., Gammie, G. F., Balbus, S. A., 1995, ApJ, 440, 742
 Hueso, R., Guillot, T., 2005, A&A, 442, 703
 Ida, S., Lin, D. N. C., 2004, ApJ, 604, 388
 Johnson, B. M., & Gammie C. F. 2003, ApJ, 597, 131
 Kratter, K. M., Matzner, Ch. D., Krumholz, M. R. 2008, ApJ, 681, 375
 Krumholz, M. R., Klein, R. I., & McKee, C. F. 2007, ApJ, 656, 959
 Laughlin, G., Bodenheimer, P., 1994, ApJ, 436, 335
 Laughlin, G., Różyczka, M., ApJ, 1996, 456, 279
 Lee, J.-E., 2007, JKAS, 40, 83
 Lin, D. N. C., Pringle, J. E., 1987, MNRAS, 225, 607
 Lin, D. N. C., Pringle, J. E., 1990, ApJ, 358, 515
 Lynden-Bell, D., Pringle, J. E., 1974, MNRAS, 168, 603
 Lodato, G., Rice, W. K. M., 2004, MNRAS, 351, 630
 Lodato, G., Rice, W. K. M., 2005, MNRAS, 358, 1489
 Lodato, G., 2007, Rivista del Nuovo Cimento, 30, 293
 Lodato, G., 2008, New Astronomy Reviews, 52, 41
 Matzner, C. D., & Levin, Yu. 2005, ApJ, 628, 817
 Mayer, L., Lufkin, G., Quinn, T., & Wadsley, J. 2007, ApJL, 661, 77
 Mejía, A. C., Durisen, R. H., Pickett, M. K., & Cai, K. 2005, ApJ, 619, 1098
 Nakamoto, T., Nakagawa, Y., 1995, ApJ, 445, 330
 Pringle, J. E., 1981, ARA&A, 19, 137
 Rice, W. K. M., Armitage, P. J., Bate, M. R., & Bonnell, I. A. 2003, MNRAS, 339, 1025
 Ruden, S. P., Pollack, J. B., 1991, ApJ, 375, 740
 Sato, T., Inutsuka, S.-I., Turner, N. J., Stone, J. M., 2004, ApJ, 605, 321
 Shakura, N. I., & Sunyaev, R. A., 1973, A&A, 24, 337
 Shu, F. H., 1977, ApJ, 214, 488
 Shu, F. H., Galli, D., Lizano, S., Glassgold, A. E., Diamond, P. H., 2007, ApJ, 665, 535
 Stamatellos, D., Hubber, D. A., & Whitworth, A. P. 2007, MNRAS, 382, L30
 Stamatellos, D., & Whitworth, A. P., 2008, A&A, 480, 879
 Stecklum, B., Melnikov, S. Y., Meusinger, H., 2007, A&A, 463, 621
 Stone, J. M., Hawley, J. F., Gammie, C. F., Balbus, S. A., 1996, ApJ, 463, 656
 Vorobyov, E. I., 2008, accepted for publication in ApJ

- Vorobyov, E. I., Basu, S., 2005, MNRAS, 360, 675
Vorobyov, E. I., Basu, S., 2005, ApJ, 633, L137
Vorobyov, E. I., Basu, S., 2006, ApJ, 650, 956
Vorobyov, E. I., Basu, S., 2007, MNRAS, 381, 1009
Vorobyov, E. I., Basu, S., 2008, ApJ, 676, L139
Young, C. H., et al., 2004, ApJS, 154, 396
Weidenschilling, S. J., 1977, Ap&SS, 51, 153